

Retraction

Retracted: Surface Feature Prediction Modeling and Parameter Optimization for Turning TC17 Titanium Alloy

International Transactions on Electrical Energy Systems

Received 28 November 2023; Accepted 28 November 2023; Published 29 November 2023

Copyright © 2023 International Transactions on Electrical Energy Systems. This is an open access article distributed under the Creative Commons Attribution License, which permits unrestricted use, distribution, and reproduction in any medium, provided the original work is properly cited.

This article has been retracted by Hindawi, as publisher, following an investigation undertaken by the publisher [1]. This investigation has uncovered evidence of systematic manipulation of the publication and peer-review process. We cannot, therefore, vouch for the reliability or integrity of this article.

Please note that this notice is intended solely to alert readers that the peer-review process of this article has been compromised.

Wiley and Hindawi regret that the usual quality checks did not identify these issues before publication and have since put additional measures in place to safeguard research integrity.

We wish to credit our Research Integrity and Research Publishing teams and anonymous and named external researchers and research integrity experts for contributing to this investigation.


The corresponding author, as the representative of all authors, has been given the opportunity to register their agreement or disagreement to this retraction. We have kept a record of any response received.

References

- [1] Z. Deng, Z. Wang, and X. Shen, "Surface Feature Prediction Modeling and Parameter Optimization for Turning TC17 Titanium Alloy," *International Transactions on Electrical Energy Systems*, vol. 2022, Article ID 2979858, 12 pages, 2022.

Research Article

Surface Feature Prediction Modeling and Parameter Optimization for Turning TC17 Titanium Alloy

Zhibo Deng,¹ Zhe Wang,² and Xuehong Shen³ 

¹Party and Government Office, Xi'an Aeronautical Polytechnic Institute, Xi'an 710089, Shaanxi, China

²Aviation Manufacturing Engineering School, Xi'an Aeronautical Polytechnic Institute, Xi'an 710089, Shaanxi, China

³School of Mechanical Engineering, Northwestern Polytechnical University, Xi'an 710072, Shaanxi, China

Correspondence should be addressed to Xuehong Shen; xhs@mail.nwpu.edu.cn

Received 18 August 2022; Revised 5 September 2022; Accepted 7 September 2022; Published 5 October 2022

Academic Editor: Nagamalai Vasimalai

Copyright © 2022 Zhibo Deng et al. This is an open access article distributed under the Creative Commons Attribution License, which permits unrestricted use, distribution, and reproduction in any medium, provided the original work is properly cited.

Surface integrity has a very significant effect on surface roughness and surface microhardness. These are the main characteristics of surface integrity. The present study investigated the influence of the cutting depth (a_p), the cutting speed (v_c), and the feed rate (f) on the surface roughness (Ra) and surface microhardness (HV) in turning TC17 titanium alloy. Data obtained from the Box-Behnken design experiments were used to develop the response surface methodology (RSM) and artificial neural network (ANN) models. Through analysis of variance (ANOVA), the relative effects of each cutting parameter on the responses have been determined. To examine the interaction effects of cutting parameters, 3D surface plots were generated. The desirability function approach (DFA) was used to optimize cutting parameters to achieve the lowest surface roughness and highest surface microhardness. The results show that ANN response prediction models have higher prediction accuracy and lower error than RSM prediction models. The optimization parameters are 60 m/min cutting speed, 0.06 mm/r feed rate, and 0.2 mm cutting depth for the minimum surface roughness and maximum surface microhardness with a maximum error of 2.83%.

1. Introduction

Titanium alloy materials have lots of advantages of high strength, good toughness, and high adaptability to forging temperature and are widely used in the manufacture of aerospace parts [1]. However, in the titanium alloy cutting process, the heat and force actions are prone to drastic changes, and the chips are very easy to adhere for causing significant tool wear [2, 3], which makes it difficult to control the concerning characteristics. It is indispensable to study the surface roughness and microhardness of titanium alloy cutting. Many professionals have conducted a large number of research on the cutting of titanium alloy materials. Mersni et al. [4] analyzed the influence of cutting speed, depth of cut, and feed per tooth on the three-dimensional surface roughness using Taguchi's method and optimized the best cutting parameters to obtain the best machining workpiece's surface. Kumar et al. [5] employed multiresponse grey relational analysis (GRA) technology to optimize process

parameters and observed the influence of cutting parameters on the surface roughness and material removal rate through the main effect diagram. Kiswanto et al. [6] used a cemented carbide tool with a diameter of 1 mm to conduct a milling experiment by changing the spindle speed and feed rate in high-speed cutting under the condition of a fixed cutting depth to measure the surface roughness under different variable combinations. They discovered that a slower cutting speed and feed rate are better for improving surface processing quality. Thirumalai et al. [7] established the quadratic regression empirical prediction model of surface roughness and cutting temperature of turning titanium alloy. Applying signal-to-noise ratio (SNR), the proportion of cutting speed on surface roughness is 38%, and the feed rate is 25%. The most important factor affecting cutting temperature is cutting speed, and the least influential factor is cutting depth. Samin et al. [8] employed Taguchi's experimental design method to carry out Ti6Al4V turning experiments. The analysis showed that the feed rate and the

TABLE 1: Chemical composition of TC17.

Element	Wt. (%)	Element	Wt. (%)
Al	5.23	Fe	0.3
Sn	1.97	C	0.05
Zr	1.9	N	0.05
Mo	4.06	H	0.01
Cr	4.04	O	0.12
Ti	Balance		

cutting depth are the most relevant parameters that affect surface roughness and cutting force. Through the turning experiments with different tool radius, Mazid et al. [9] obtained the optimized parameter range of surface roughness from $0.5\ \mu\text{m}$ to $1\ \mu\text{m}$ based on a cutting speed of 60–250 m/min, the feed speed 0.1 mm/r and the cutting depth 0.5 mm. Matras et al. [10] put forward that the influence of cutting speed on surface roughness can be ignored, and it takes the minimum surface roughness as the objective to optimize the process parameters. Seung et al. [11] analyzed the impact of machining tools on the machinability of titanium alloy. The consequences show that the dynamic range of cutting force and surface roughness of coated cemented carbide tool and cermet tool is larger than cemented carbide tool, and the influencing factors of tool life are tool material, cutting speed, and feed. By studying the influence of tool microstructure on chip morphology, cutting force, surface state, and surface roughness, Qian et al. [12] analyzed and summarized the test data and found that the key factor to improve the machinability of TC21 titanium alloy was the microstructure. Besides, scholars pay attention to the tool wear because the material is easy to stick to the tool in the process of titanium alloy. Aramcharoen [13] found that low-temperature cooling can reduce friction between the tool and the chip, improve production efficiency and tool life, and create a thinner secondary deformation zone. Taking 0.1 mm as the tool wear limit, Priarone et al. [14] proposed that low-temperature cooling can extend the tool life of uncoated cemented carbide tools by 2 minutes, CBN tools about 7.2 minutes, and PCD tools with different grain sizes by 14 minutes compared with traditional oil cooling and low-temperature cooling. With the emergence of new processing methods, Che-Haron [15] carried out the cutting experiments of Ti-6Al-2Sn-4Zr-6Mo with different grain sizes ($1.0\ \mu\text{m}$ and $0.68\ \mu\text{m}$) uncoated cemented carbide tools to describe that the main forms of tool wear are excessive cutting. Furthermore, it is stated that the finer the grain size, the longer is the tool life. Muhammad et al. [16] used unified Ti6Al4V turning experiments to analyze tool wear and energy distributions to evaluate the tool wear rate and energy generated by different cutting conditions. Due to the large contact length and high chip compression ratio, serious tool wear and a large energy zone appear in high-speed cutting.

At present, the research on titanium alloy mainly focuses on Ti6Al4V. Compared with others, the TC17 has bigger yield strength, smaller elongation, and lower elasticity modulus. The research on TC17 titanium alloy is still relatively very lacking. Therefore, it is necessary to study the surface roughness and surface microhardness of turning

TABLE 2: Material properties of TC17.

Material properties	Value
Elastic modulus	112 (GPa)
Tensile strength	1960 (MPa)
Yield strength	1890 (MPa)
Density	$4.55\ (\text{g}/\text{cm}^3)$
Hardness	41 (HRC)
Elastic modulus	112 (GPa)
Tensile strength	1960 (MPa)

TABLE 3: Chosen parameters and levels.

Code	Experimental factors	Units	Levels		
			1	2	3
A	Cutting speed	m/min	30	60	90
B	Feed rate	mm/r	0.06	0.12	0.18
C	Cutting depth	mm	0.1	0.2	0.3

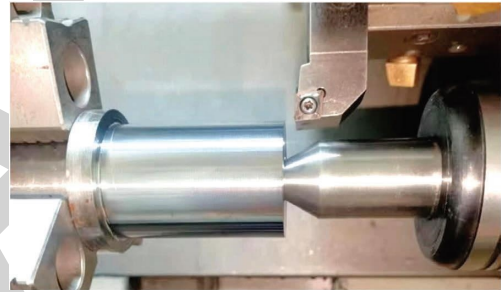


FIGURE 1: The experimental conditions.

TC17. The results can conduct the selection of cutting parameters according to the application requirements.

2. Experimental Conditions and Methods

The experimental material is titanium alloy TC17, which is an $\alpha+\beta$ dual-phase alloy rich in α phase. Its chemical composition is depicted in Table 1, and its fundamental material properties are presented in Table 2 [17, 18]. The experimental piece is $\Phi 60\ \text{mm} \times 280\ \text{mm}$ bar material. The tool model is a hard alloy tool YG6, with a rake angle of 6° , and a relief angle of 10° . In order to reduce the cutting temperature, a large amount of cutting fluid with a cooling effect should be poured into the cutting area. Because the thermal conductivity of titanium alloy is low, which is only 1/7 of steel and 1/6 of aluminum, the heat can't be quickly transferred with the chips in the machining process. When turning and cutting titanium alloys, emulsions or water-soluble cutting fluids with extreme pressure additives are often used, which is not easy to reach the ignition temperature. It is better not to use gaseous coolant in titanium alloy processing, so as to avoid toxic substances and hydrogen embrittlement and also prevent high-temperature stress corrosion cracking of titanium alloy. In this experiment, the emulsion is selected for cooling. According to the actual processing conditions. To reduce the interference of other nonconcerned factors on the reliability of the

TABLE 4: The response surface experimental results.

No.	Cutting speed v_c (m/min)	Feed rate f (mm/r)	Cutting depth a_p (mm)	Surface roughness Ra (μm)	Surface microhardness HV
1	60	0.12	0.2	1.36	455
2	30	0.06	0.3	0.79	435
3	60	0.12	0.2	1.28	460
4	90	0.06	0.1	0.7	438
5	30	0.06	0.1	0.68	440
6	90	0.18	0.3	2.51	449
7	60	0.18	0.2	2.17	450
8	60	0.06	0.2	0.74	456
9	90	0.18	0.1	1.81	412
10	60	0.12	0.1	1.35	440
11	60	0.12	0.2	1.32	458
12	60	0.12	0.2	1.2	449
13	90	0.06	0.3	0.83	421
14	30	0.12	0.2	1.58	426
15	90	0.12	0.2	1.37	420
16	30	0.18	0.3	2.32	480
17	60	0.12	0.2	1.45	452
18	60	0.12	0.3	1.53	468
19	60	0.12	0.2	1.21	448
20	30	0.18	0.1	2.27	426

TABLE 5: Analysis of variance for Ra .

Source	DF	Adj SS	Adj MS	F-value	P-value	C. (%)	Signif
Model	9	5.74	0.64	45.52	<0.0001	97.62	YES
A	1	0.018	0.018	1.26	0.288	0.31	
B	1	5.39	5.39	384.57	<0.0001	91.67	
C	1	0.14	0.14	9.77	0.0108	2.38	
AB	1	0.014	0.014	0.97	0.3475	0.24	
AC	1	0.056	0.056	4.01	0.0732	0.95	
BC	1	0.033	0.033	2.32	0.1586	0.56	
A^2	1	0.014	0.014	1.01	0.338	0.24	
B^2	1	7.38E-03	7.38E-03	0.53	0.4845	0.13	
C^2	1	3.73E-03	3.73E-03	0.27	0.6172	0.06	
Error	10	0.14	0.014				
Total	19	5.88					

experimental results, each set of experiments adopts a new blade. Using the Box-Behnken design experimental program [19], which is shown in Table 3, to plan the experiment with cutting speed, feed, and cutting depth as experimental factors with three levels defined for each factor.

The length of processing for each set of parameters is 10 millimeters. Figure 1 illustrates the experimental conditions. The experimental results are surface roughness (Ra) and surface microhardness (HV), which were measured using the conventional surface roughness tester TR240 and the digital display Micro Vickers hardness tester HV-50, respectively. To reduce measurement error, the average of three measurements is applied to each result. Table 4 represents the precise experimental arrangement and measurement data.

3. Prediction Model and Influence Law

3.1. Analysis of Variance (ANOVA). Analysis of variance (ANOVA) is one method for assessing the significance of input factors on response variables. In addition, it is a

TABLE 6: Analysis of variance for HV.

Source	DF	Adj SS	Adj MS	F-value	P-value	C. (%)	Signif
Model	9	5300.78	588.98	15.51	<0.0001	93.31	YES
A	1	448.9	448.9	11.82	0.0064	7.90	
B	1	72.9	72.9	1.92	0.196	1.28	
C	1	940.9	940.9	24.78	0.0006	16.56	
AB	1	105.12	105.12	2.77	0.1271	1.85	
AC	1	105.12	105.12	2.77	0.1271	1.85	
BC	1	1596.13	1596.13	42.03	<0.0001	28.10	
A^2	1	1750.14	1750.14	46.08	<0.0001	30.81	
B^2	1	62.64	62.64	1.65	0.228	1.10	
C^2	1	91.64	91.64	2.41	0.1514	1.61	
Error	10						
Total	19						

convenient and swift solution process that is widely accepted and utilized. Table 5 are the results of ANOVA for surface roughness (Ra). In Table 5, the P-Value does not exceed 0.05, which indicates that the influence of the input

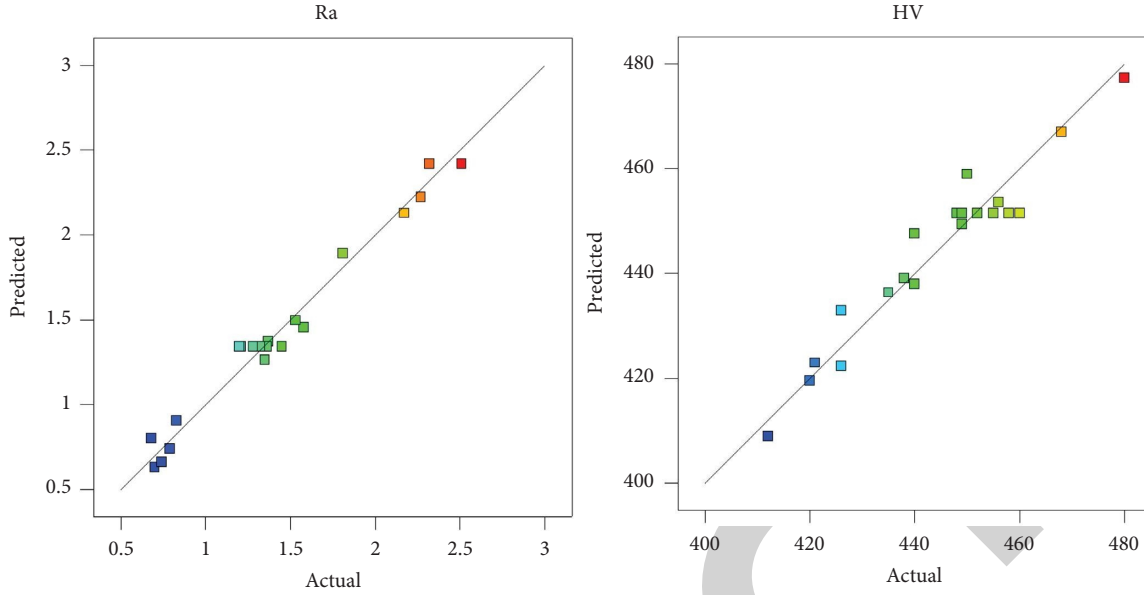


FIGURE 2: Comparison of prediction models for Ra and HV .

parameters is established, and the cutting parameters play a key role in surface roughness. The A , B , and C input parameters expend percentages for surface roughness (Ra) are 0.31%, 91.67%, and 2.38% respectively. It indicates that B has the principal influence on the surface roughness (Ra), shortly followed by C . The P -Value of A to surface roughness (Ra) is greater than 0.05, indicating that it can be ignored.

For the surface microhardness (HV), the ANOVA results are shown in Table 6. Through analysis, the percentage contributions of process parameters for A , B , and C were defined as (7.90%, 1.28%, and 16.56%), respectively. It shows that C with 16.56% contributions occupies the first position in influencing surface microhardness (HV). The next factor is A with 7.90% contributions. For the low contribution of B (1.28%), it shows that B has no significant influence on the surface microhardness (HV).

3.2. Response Surface Method(RSM) Modeling Development

3.2.1. Regression Analysis. Regression analysis is based on a large number of test data analysis results, using mathematical methods to establish the relationship model between input variables and output variables. It can be used to predict the value of the variable and is widely used in industrial production and science research. The response surface method (RSM) is a test method that considers interference factors and is accepted by the public [20, 21]. The regression model obtained through experimental design can be expressed as in the following Equation:

$$y = \beta_0 + \sum_{i=1}^m \beta_i x_i + \sum_{i=1}^m \beta_{ii} x_i^2 + \sum_{i < j} \beta_{ij} x_i x_j, \quad (1)$$

where, β_0 is the constant term, β_i is the linear effect of x_i , β_{ii} is the second-order effect of x_i , β_{ij} is the interactive effect between x_i and x_j , and x_i and x_j are the input and response variables, respectively.

Equations (2) and (3) can be used to calculate prediction models for surface roughness (Ra) and surface microhardness (HV) (3).

$$\begin{aligned} Ra = & 0.792 - 0.01v_c + 8.02f - 3.25a_p \\ & - 0.02v_c f + 0.02v_c a_p + 10.06f a_p \\ & + 0.00007v_c^2 + 14.39f^2 + 3.68a_p^2 \end{aligned} \quad (2)$$

$$R^2 = 0.9762,$$

$$\begin{aligned} HV = & 408.86 + 3.62v_c - 623.18f - 343.90a_p \\ & - 2.01v_c f - 1.21v_c a_p + 2354.16f a_p \\ & - 0.02v_c^2 + 1325.75f^2 + 577.27a_p^2 \end{aligned} \quad (3)$$

$$R^2 = 0.9331.$$

The correlation coefficients R^2 of the regression equations that advanced for the predictive surface roughness and surface microhardness were computed as $R^2 = 98\%$ and $R^2 = 93\%$, respectively. Figure 2 depicts a comparison of experimental results and predicted values obtained from regression equations. Most of the true values are scattered on the predicted value, and a small part of the true values are scattered on both sides of the predicted value, indicating that the model fits well with the actual results. As a result, the regression model can estimate the surface feature, including Ra and HV .

3.2.2. Surface Plot in 3D. Figure 3 shows the variation of Ra with the interaction of machining process factors. The cutting depth in Figure 3(a) is 0.2 mm. The surface roughness increases linearly as the feed rate (f) increases

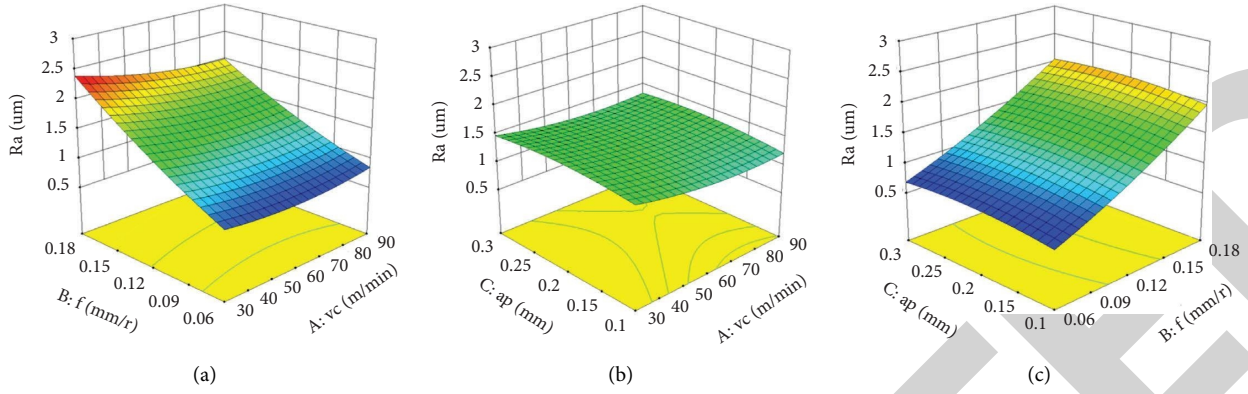


FIGURE 3: The influence of the machining factor on R_a . (a) Interaction of f and v_c on R_a , (b) interaction of a_p and v_c on R_a , and (c) interaction of a_p and f on R_a .

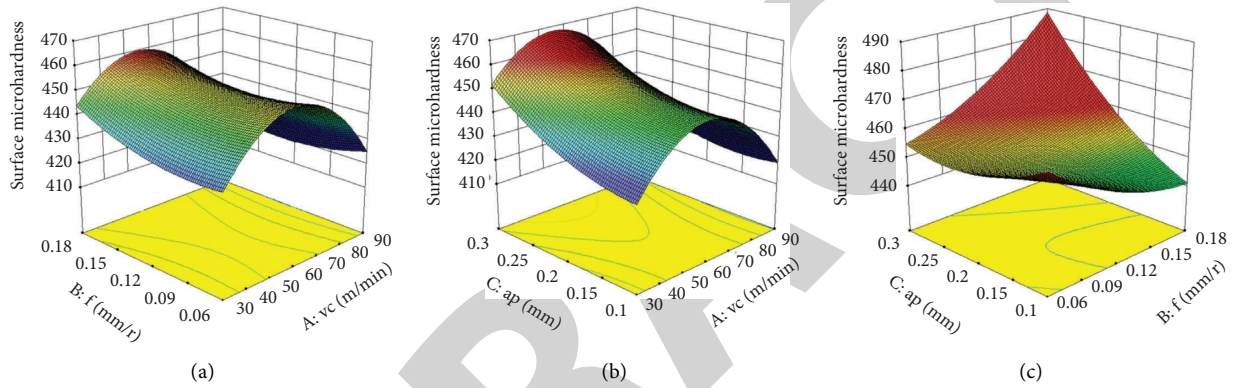


FIGURE 4: The influence of cutting parameters on HV . (a) The influence of f and v_c on HV . (b) The influence of a_p and v_c on HV . (c) The influence of a_p and f on HV .

from 0.06 mm/r to 0.18 mm/r. The effect of cutting speed on the R_a is less than the feed rate. The roughness is at its worst state level when the feed rate and cutting speed are both set to low levels.

The interaction of cutting speed and cutting depth on R_a is illustrated in Figure 3(b). In this analysis, the feed rate is selected by 0.12 mm/r, and the fluctuation range of R_a is from 1.2 to 1.6 μm . It has been discovered that both the cutting depth and the cutting speed have some very slight effects on the R_a . The R_a response surface graph of the cutting depth and feed rate at a cutting speed of 60 m/min is shown in Figure 3(c). In contrast, R_a is susceptible to feed rate fluctuations and less susceptible to cutting depth. The R_a reaches the maximum value of 2.4 μm with the machining parameter factor cutting speed which is 60 m/min, the feed rate is 0.18 mm/r, and the cutting depth is 0.3 mm.

The 3D plot of milling parameters on surface microhardness (HV) was presented in Figure 4. In Figure 4(a), while the feed goes up from the initial value of 0.06 mm/r to 0.18 mm/r, the maximum surface microhardness is obtained at $v_c = 70$ m/min. Figure 4(b) demonstrates that the surface microhardness rises with increasing cutting depth. Figure 4(c) demonstrates that the cutting depth continuously increases from 0.1 to 0.3 mm, while the microhardness decreases. The maximum microhardness value can be

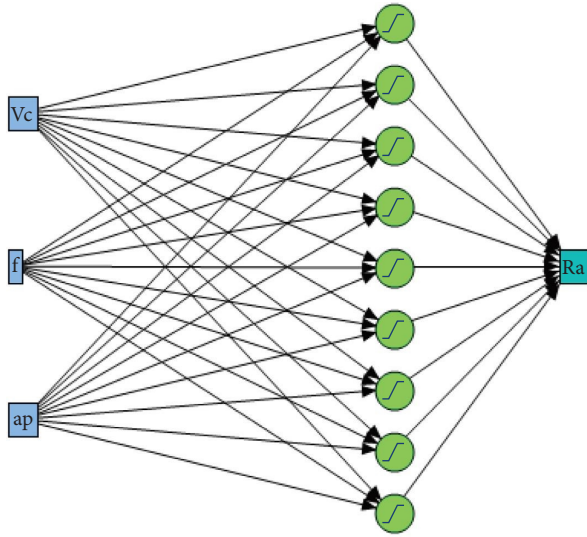
obtained under the condition of large feed and large cutting depth, up to nearly 490 HV . It can be seen from the interaction depicted and contour diagram of the comprehensive response surface that microhardness is sensitive to feed rate and cutting depth, which is consistent with the coefficient reflection of the established model.

4. Artificial Neural Network (ANN)

Compared with the regression analysis, the artificial neural network (ANN) does not need to specify the mathematical model in advance, which avoids the shortcomings of the curve fitting method and improves the prediction modeling accuracy. ANN is widely used in prediction, classification, and other research due to its self-learning and self-adaptive advantages in processing random data and nonlinear data. Maheshwera et al. [22] used regression analysis and artificial neural network models to predict the R_a of AISI 52100 steel during hard turning. The difference between the calculated values of the model and the experimental results is particularly small. Using the ANN, Abbas et al. [23] successfully predicted the surface roughness of AZ61 magnesium alloy final turning with an accuracy of 1.35%. For the drilling process, Kolesnyk et al. [24] selected ANN to research CFRP/Ti alloy material and analyzed the cutting heat

TABLE 7: Performance of ANN structure of Ra .

Inp_Hid_Oup	Root mean square error (RMSE)	Coefficient of determination (R^2)
3-5-1	0.0508	0.9871
3-6-1	0.0886	0.9607
3-7-1	0.0881	0.9611
3-8-1	0.0504	0.9873
3-9-1	0.0171	0.9999
3-10-1	0.0818	0.9665

FIGURE 5: The optimal network structure for Ra .

generated in the drilling process and the surface quality of the workpiece after drilling. The results show that ANN can be used to identify the drilling parameter-hole quality relationship. Sangwan et al. [25] and Kumar and Chauhan [26] proposed a method combining ANN and genetic algorithm to optimize the turning machining factors. It can be seen

from the above research works that using the ANN model to examine the nonlinear relationship between the virtual machining parameters and the machining performance is effective in predicting the actual machining process.

The structure of the neural network can be defined as 3- H -1, which stands for three input parameters (cutting speed, feed rate, and cutting depth) with H number of hidden layer nodes and one response (surface roughness or surface microhardness). The excitation function of the neural network adopts the hyperbolic tangent function (TanH) [27], which transforms values to be between -1 and 1 and its expression is given in the following Equation:

$$\text{TanH} = \frac{e^{2x} - 1}{e^{2x} + 1} \quad (4)$$

4.1. Application of ANN to Model (Ra). According to Table 7, some ANN structures were tested. Figure 5 depicts the best network topology, which is 3-9-1 based on a smaller RMSE and a higher R^2 . It is made up of three input layer nodes, nine hidden layer nodes, and one output layer node with a linear transfer function.

The mathematical model for surface roughness (Ra) derived by the ANN approach is shown in the following Equation with $R^2 = 99.99\%$:

$$\begin{aligned} Ra = & 1.9478 - 0.4451 * H1 + 1.7919 * H2 - 1.5120 * H3 + 3.1112 * H4 \\ & - 0.4457 * H5 + 0.5689 * H6 + 0.7477 * H7 + 3.1521 * H8 - 0.47247 * H9, \end{aligned} \quad (5)$$

where,

$$\begin{aligned} H1 &= \text{TanH}(3.4307 + -6.5460 * ap + 8.7363 * f + -0.04552 * Vc), \\ H2 &= \text{TanH}(1.4897 + 1.6920 * ap + -15.8407 * f + 0.0022 * Vc), \\ H3 &= \text{TanH}(-3.6149 + 8.3069 * ap + 6.0278 * f + 0.01098 * Vc), \\ H4 &= \text{TanH}(-2.59039 + 7.2156 * ap + 3.4107 * f + 0.0076 * Vc), \\ H5 &= \text{TanH}(3.5705 - 2.3971 * ap + -15.6305 * f + -0.02977 * Vc), \\ H6 &= \text{TanH}(-2.8044 + 0.1261 * ap + 7.1547 * f + 0.0197 * Vc), \\ H7 &= \text{TanH}(-0.5712 + -3.5080 * ap + 10.1420 * f + 0.01147 * Vc), \\ H8 &= \text{TanH}(1.7555 + -2.8133 * ap + -5.9964 * f + -0.0103 * Vc), \\ H9 &= \text{TanH}(-3.9836 - 1.9689 * ap + 20.2767 * f + 0.03528 * Vc), \end{aligned} \quad (6)$$

4.2. *Application of ANN to Model (HV)*. In the same way, the test results of the several ANN architectures of *HV* are shown in Table 8. The architecture chosen is 3-10-1 (Figure 6) with the highest R^2 and the lowest RMSE.

The mathematical model obtained by the ANN method for the surface microhardness (*HV*) is expressed in the following Equation with $R^2 = 99.23\%$:

TABLE 8: Performance of ANN structure of HV.

Inp_Hid_Oup	RMSE	R^2
3-5-1	11.3270	0.6309
3-6-1	103005	0.6947
3-7-1	2.3532	0.9840
3-8-1	10.2615	0.6970
3-9-1	2.3882	0.9835
3-10-1	1.6329	0.9923

$$\begin{aligned}
 HV = & 425.8282 + 25.4849 * H1 + 1.8094 * H10 + 298.8565 * H2 \\
 & + 41.14935 * H3 - 22.76606 * H4 - 122.02144 * H5 \\
 & - 19.6225 * H6 - 158.3730 * H7 - 38.6868 * H8 - 136.0233 * H9,
 \end{aligned} \tag{7}$$

where,

$$\begin{aligned}
 H1 &= \text{TanH}(3.3995 - 8.1659 * ap - 3.0219 * f - 0.0270 * Vc), \\
 H2 &= \text{TanH}(-2.7765 + 5.2553 * ap + 3.6597 * f + 0.0102 * Vc), \\
 H3 &= \text{TanH}(1.8557 + 3.7416 * ap - 17.2210 * f - 0.0135 * Vc), \\
 H4 &= \text{TanH}(2.2312 - 11.05189 * ap - 1.0593 * f - 0.0057 * Vc), \\
 H5 &= \text{TanH}(-3.4709 + 7.0627 * ap - 3.4015 * f + 0.02637 * Vc), \\
 H6 &= \text{TanH}(-6.0225 + 8.4248 * ap + 25.9316 * f + 0.02868 * Vc), \\
 H7 &= \text{TanH}(-3.2211 + 3.0372 * ap + 7.5765 * f + 0.01766 * Vc), \\
 H8 &= \text{TanH}(5.2797 - 3.4336 * ap - 24.5623 * f - 0.02859 * Vc), \\
 H9 &= \text{TanH}(0.17486 + 2.9591 * ap - 1.5697 * f - 0.0149 * Vc), \\
 H10 &= \text{TanH}(-2.6185 + 1.1293 * ap + 16.5582 * f + 0.01407 * Vc).
 \end{aligned} \tag{8}$$

Table 9 and Figures 7 and 8 are the comparison of experimental and estimated by RSM and ANN, and the absolute percentage error (Δ) is calculated using the following Equation [22]:

$$\Delta = \left| \frac{y_{\text{exp}} - y_{\text{pred}}}{y_{\text{exp}}} \right| \times 100\%. \tag{9}$$

For RSM and ANN, the maximum test errors for surface roughness are about 30.02% and 11.78%, respectively. The mean absolute percentage error between RSM and experimental values can be seen as 9.50%, whereas the same value is only 3.48% with the ANN model. In surface microhardness, the same maximum test errors for RSM and ANN are revealed as 15.84% and 3.22%, respectively. The mean absolute percentage

errors between experimental and estimated by RSM and ANN are found to be 7.36% and 0.85%. Actual values and anticipated values for ANN and RSM are shown in Figures 7 and 8. Thus, it can be seen that ANN is closer to the test results than RSM, showing a better fitting effect.

5. Optimization with DFA

One of the most popular approaches for manufacturing's multiple response process optimizations is the desire function approach (DFA) [28, 29]. A typical way is the desirability approach, which allocates a "score" to a collection of replies and selects factor settings that maximizes that score. To find out the maximum and minimum of the target goal, the desirability can be defined from the following Equations:

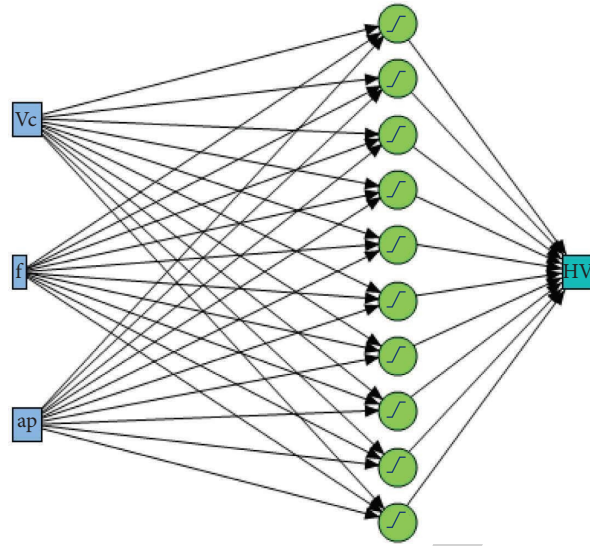


FIGURE 6: The optimal network structure for HV.

TABLE 9: Comparison of the measured and predicted value.

No.	R_a (μm) exp	Surface roughness (R_a)				HV (%) exp	Surface microhardness (HV)			
		RSM pred	ANN pred	Error (%) (RSM)	Error (%) (ANN)		RSM pred	ANN pred	Error (%) (RSM)	Error (%) (ANN)
1	1.36	1.4483	1.3414	6.49	1.37	455	480.1878	455.8414	5.54	0.18
2	0.79	0.7693	0.7919	2.62	0.24	435	443.4931	434.5498	1.95	0.10
3	1.28	1.4483	1.3414	13.15	4.80	460	480.1878	455.8414	4.39	0.90
4	0.7	0.8362	0.7289	19.45	4.12	438	503.8056	437.634	15.02	0.08
5	0.68	0.8842	0.6828	30.02	0.41	440	445.1016	439.8475	1.16	0.03
6	2.51	2.4843	2.6508	1.02	5.61	449	514.1188	447.0804	14.50	0.43
7	2.17	2.2372	1.9451	3.10	10.37	450	487.6745	461.8817	8.37	2.64
8	0.74	0.7629	0.7444	3.10	0.60	456	482.2466	455.3319	5.76	0.15
9	1.81	2.1177	1.8151	17.00	0.28	412	473.7475	410.6579	14.99	0.33
10	1.35	1.4221	1.3597	5.34	0.72	440	476.2698	454.162	8.24	3.22
11	1.32	1.4483	1.3414	9.72	1.62	458	480.1878	455.8414	4.84	0.47
12	1.2	1.4483	1.3414	20.69	11.78	449	480.1878	455.8414	6.95	1.52
13	0.83	0.9613	0.8347	15.82	0.57	421	487.6771	418.8745	15.84	0.50
14	1.58	1.5113	1.5847	4.35	0.30	426	440.0838	434.1304	3.31	1.91
15	1.37	1.5113	1.3815	10.31	0.84	420	484.2918	418.2745	15.31	0.41
16	2.32	2.4363	2.3226	5.01	0.11	480	484.4068	479.3656	0.92	0.13
17	1.45	1.4483	1.3414	0.12	7.49	452	480.1878	455.8414	6.24	0.85
18	1.53	1.5480	1.4374	1.17	6.05	468	495.6513	462.1011	5.91	1.26
19	1.21	1.4483	1.3414	19.69	10.86	448	480.1878	455.8414	7.18	1.75
20	2.27	2.3097	2.3047	1.75	1.53	426	429.5155	425.728	0.83	0.06
Average				9.50	3.48				7.36	0.85

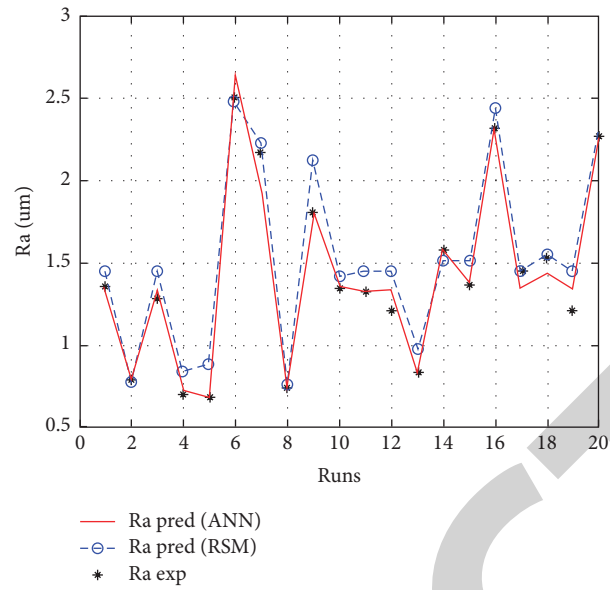
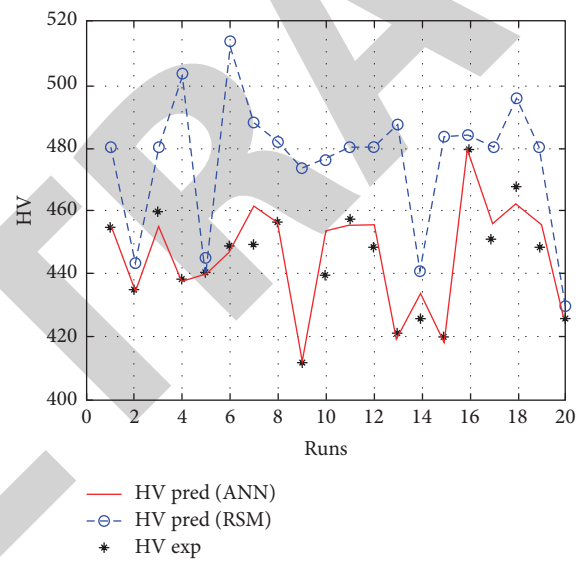
FIGURE 7: Experimental, RSM, and ANN predicted results for Ra .FIGURE 8: Experimental, RSM, and ANN predicted results for HV .

TABLE 10: Expectation assessment for Ra and HV .

Runs.	ANN predicted value ($y_{i,p}$)		Individual desirability (d_i)		Composite desirability (Des_{comb}) (%)	Rank
	Ra	HV	Ra (%)	HV (%)		
1	1.3414	455.8414	0.6654	0.6576	0.6615	3
2	0.7919	434.5498	0.9446	0.3477	0.5731	12
3	1.3414	455.8414	0.6654	0.6576	0.6615	3
4	0.7289	437.6340	0.9766	0.3926	0.6192	11
5	0.6828	439.8475	1.0000	0.4248	0.6518	9
6	2.6508	447.0804	0.0000	0.5301	0.0000	19
7	1.9451	461.8817	0.3586	0.7455	0.5171	13
8	0.7444	455.3319	0.9687	0.6502	0.7936	1
9	1.8151	410.6579	0.4246	0.0000	0.0000	19
10	1.3597	454.1620	0.6560	0.6332	0.6445	10
11	1.3414	455.8414	0.6654	0.6576	0.6615	3
12	1.3414	455.8414	0.6654	0.6576	0.6615	3
13	0.8347	418.8745	0.9228	0.1196	0.3322	16
14	1.5847	434.1304	0.5417	0.3416	0.4302	14
15	1.3815	418.2745	0.6450	0.1109	0.2674	17
16	2.3226	479.3656	0.1668	1.0000	0.4084	15
17	1.3414	455.8414	0.6654	0.6576	0.6615	3
18	1.4374	462.1011	0.6166	0.7487	0.6795	2
19	1.3414	455.8414	0.6654	0.6576	0.6615	3
20	2.3047	425.7280	0.1759	0.2193	0.1964	18

TABLE 11: Confirmation of optimization results.

Responses	Predicted ($v_{c2-f1-a_p2}$)	Experimental ($v_{c2-f1-a_p2}$)	Error (%)
Ra (μm)	0.7444	0.751	0.89
HV	455.3319	468.2	2.83

desirability. It is expected that the individual desirability of surface roughness is smaller the better and surface microhardness is larger the better, which were calculated by Equations (10) and (11) respectively. Table 10 shows the evaluated individual and composite desirability, as well as their rank for (Ra) and (HV). The optimization parameters are $v_{c2-f1-a_p2}$, which are cutting speed = 60 m/min, feed rate = 0.06 mm/r, and cutting depth = 0.2 mm with estimated $Ra = 0.7444\mu\text{m}$ and surface microhardness $HV = 455.3319$.

$$d_i = \begin{cases} 0, & \text{if } y_{i,p} \leq y_{i,p,\min} \\ \frac{y_{i,p,\max} - y_{i,p}}{y_{i,p,\max} - y_{i,p,\min}}, & \text{if } y_{i,p,\min} \leq y_{i,p} \leq y_{i,p,\max} \\ 1, & \text{if } y_{i,p} \geq y_{i,p,\max} \end{cases} \quad (10)$$

$$d_i = \begin{cases} 0, & \text{if } y_{i,p} \leq y_{i,p,\min} \\ \frac{y_{i,p} - y_{i,p,\min}}{y_{i,p,\max} - y_{i,p,\min}}, & \text{if } y_{i,p,\min} \leq y_{i,p} \leq y_{i,p,\max} \\ 1, & \text{if } y_{i,p} \geq y_{i,p,\max} \end{cases} \quad (11)$$

$$Des_{comb} = \left(\prod_{i=1}^n d_i \right)^{(1/n)}, \quad (12)$$

where, d_i is the individual desirability and $y_{i,p}$ is the response, $y_{i,p,\max}$ and $y_{i,p,\min}$ are the max and the min values of the response. n is the number of responses. Des_{comb} is the composite desirability, which gets all goals combined into one desirability function.

According to the previous analysis, ANN models with reliable predictability are used to evaluate individual

6. Confirmation Test

To verify the reliability of the optimization results, the optimized parameters of $v_{c2-f1-a_p2}$ were selected for the confirmation experiment (seen in Table 11). The surface roughness and surface microhardness obtained by the test were $0.751\mu\text{m}$ and 468.2 . The error rates are about 0.89% and 2.83% between the predicted and experimental, which can prove the reliability of the optimization results.

7. Conclusions

In this paper, the predicted models of surface roughness and surface microhardness are established using RSM and ANN techniques in the TC17 turning experiment based on the Box-Behnken design, and the following conclusions can be obtained:

- (1) From the ANOVA analysis, feed rate with 91.67% contributions has the most important influence on the surface roughness (Ra) and cutting depth with 16.56% contributions occupies the first position in influencing the quality of surface microhardness (HV).

- (2) The ANN prediction models of surface roughness ($R^2 = 99.99\%$) and surface microhardness ($R^2 = 99.23\%$) have higher prediction accuracy and small error than the RSM prediction models of surface roughness ($R^2 = 97.62\%$) and surface microhardness ($R^2 = 93.31\%$).
- (3) The mean absolute percentage errors for Ra and HV between experimental and estimated by ANN can be only 3.48% and 0.85%, which are smaller than 9.50% and 7.36% estimated by RSM.
- (4) The optimization parameters with minimum surface roughness and maximize surface microhardness are cutting speed 60 m/min, feed rate 0.06 mm/r, and cutting depth 0.2 mm, which were obtained with the DFA technique. In the confirmed experiment, the errors of Ra and HV between ANN predicted and the experiment are 0.89% and 2.83%.

Data Availability

The data of this paper can be obtained through the e-mail to the authors.

Conflicts of Interest

The authors declare that they have no conflicts of interest.

Authors' Contributions

Z. D. and Z. W. performed data curation; Z. W. and X. S. performed investigation; Z. W. developed the methodology; Z. W. wrote the original draft; Z. D. and X. S. reviewed and edited the study. All authors have read and agreed to the published version of the manuscript.

Acknowledgments

This study was supported by Natural Science Basic Research Program of Shaanxi (Program No. 2022JM-304) and Scientific Research Program Funded by Education Department of Shaanxi Provincial Government (Program No. 22JK0428).

References

- [1] M. Rahman, Y. S. Wong, and A. R. Zareena, "Machinability of titanium alloys," *JSME International Journal Series C*, vol. 46, no. 1, pp. 107–115, 2003.
- [2] T. Liang, Z. Dinghua, and Y. Changfeng, "Effect of high-speed milling parameters on surface metamorphic layer of TC17 titanium alloy," *Journal of Aeronautical Materials*, vol. 37, pp. 75–81, 2017.
- [3] L. Liyun, W. Jinfang, and T. Zhibiao, "Study on the roughness of the machined surface and wear mechanism of the cutter in dry cutting aluminum alloy with YG8 cemented carbide," *Technology and Test*, vol. 6, pp. 120–123, 2018.
- [4] W. Mersni, M. Boujelbene, S. B. Salem, and A. S. Alghamdi, "Optimization of the surface roughness in ball end milling of titanium alloy Ti-6Al-4V using the Taguchi Method," *Procedia Manufacturing*, vol. 20, pp. 271–276, 2018.
- [5] R. Kumar, S. Roy, P. Gunjan, A. Sahoo, D. D. Sarkar, and R. K. Das, "Analysis of MRR and surface roughness in machining Ti-6Al-4V ELI titanium alloy using EDM process," *Procedia Manufacturing*, vol. 20, pp. 358–364, 2018.
- [6] G. Kiswanto, A. Mandala, M. Azmi, and T. J. Ko, "The effects of cutting parameters to the surface roughness in high speed cutting of micro-milling titanium alloy Ti-6Al-4V," *Key Engineering Materials*, vol. 846, pp. 133–138, 2020.
- [7] R. Thirumalai, K. Techato, M. Chandrasekaran, K. Venkatapathy, and M. Seenivasan, "Experimental investigation during turning process of titanium material for surface roughness," *Materials Today Proceedings*, vol. 45, pp. 1423–1426, 2021.
- [8] R. Samin, M. Z. Nuawi, and S. M. Haris, "Optimization of the surface roughness for titanium Ti6Al4V in turning process using Taguchi method," *Test Engineering and Management*, vol. 83, pp. 1072–1078, 2020.
- [9] A. M. Mazid, M. S. Hasan, and K. B. Ahsan, "An investigation on optimum process parameters in terms of surface roughness for turning titanium alloy Ti-6Al-4V using coated carbide," *International Journal of Engineering Materials and Manufacture*, vol. 4, pp. 137–145, 2019.
- [10] A. Matras, W. Zbala, and M. Machno, "Research and method of roughness prediction of a curvilinear surface after titanium alloy turning," *Materials*, vol. 12, pp. 1–14, 2019.
- [11] H. Y. Seung, H. L. Jeong, and H. O. Sung, "A study on cutting characteristics in turning operations of titanium alloy used in automobile," *International Journal of Precision Engineering and Manufacturing*, vol. 20, pp. 209–216, 2019.
- [12] X. Qian, X. Duan, and J. Zou, "Effects of different tool microstructures on the precision turning of titanium alloy TC21," *International Journal of Advanced Manufacturing Technology*, vol. 106, no. 11–12, pp. 5519–5526, 2020.
- [13] A. Aramcharoen, "Influence of cryogenic cooling on tool wear and chip formation in turning of titanium alloy," *Procedia CIRP*, vol. 46, pp. 83–86, 2016.
- [14] P. C. Priarone, F. Klocke, M. G. Faga, D. Lung, and L. Settineri, "Tool life and surface integrity when turning titanium aluminides with PCD tools under conventional wet cutting and cryogenic cooling," *International Journal of Advanced Manufacturing Technology*, vol. 85, no. 1–4, pp. 807–816, 2016.
- [15] C. H. Che-Haron, "Tool life and surface integrity in turning titanium alloy," *Journal of Materials Processing Technology*, vol. 118, no. 1–3, pp. 231–237, 2001.
- [16] Y. Muhammad, H. I. Syed, A. K. Jaffery, and K. Mushtaq, "Development and analysis of tool wear and energy consumption maps for turning of titanium alloy (Ti6Al4V)," *Journal of Manufacturing Processes*, vol. 62, pp. 613–622, 2021.
- [17] X. Shen, D. Zhang, C. Yao, L. Tan, and H. Yao, "Formation mechanism of surface metamorphic layer and influence rule on milling TC17 titanium alloy," *International Journal of Advanced Manufacturing Technology*, vol. 6, pp. 1–18, 2021.
- [18] X. Shen, D. Zhang, and L. Tan, "Effects of cutter path orientations on milling force, temperature, and surface integrity when ball end milling of TC17 alloy," *Proceedings of the Institution of Mechanical Engineers-Part B: Journal of Engineering Manufacture*, vol. 7, Article ID 095440542097107, 2020.
- [19] L. Zhanqiang and A. Xin, "Investigation of wear lifespan of cutting tools in high-speed machining," *Tool Engineering*, vol. 12, pp. 3–7, 2001.

- [20] Y. Ming, "Minitab for central composite design and data processing," *Pharmaceutical Care and Research*, vol. 007, pp. 231–234, 2007.
- [21] B. C. Routara, A. K. Sahoo, A. K. Parida, and P. Padhi, "Response surface methodology and genetic algorithm used to optimize the cutting condition for surface roughness parameters in CNC turning," *Procedia Engineering*, vol. 38, pp. 1893–1904, 2012.
- [22] U. Maheshwera Reddy Paturi, H. Devarasetti, and S. Kumar Reddy Narala, "Application of regression and artificial neural network analysis in modelling of surface roughness in hard turning of AISI 52100 steel," *Materials Today Proceedings*, vol. 5, no. 2, pp. 4766–4777, 2018.
- [23] A. T. Abbas, D. Y. Pimenov, I. N. Erdakov, M. A. Taha, M. S. Soliman, and M. M. El Rayes, "ANN surface roughness optimization of AZ61 Magnesium alloy finish turning: minimum machining times at prime machining costs," *Materials*, vol. 11, no. 5, p. 808, 2018.
- [24] V. Kolesnyk, J. Peterka, O. I. Alekseev et al., "Application of ANN for analysis of hole accuracy and drilling temperature when drilling CFRP/Ti alloy stacks," *Materials*, vol. 15, no. 5, p. 1940, 2022.
- [25] K. S. Sangwan, S. Saxena, and G. Kant, "Optimization of machining parameters to minimize surface roughness using integrated ANN-GA approach," *Procedia CIRP*, vol. 29, pp. 305–310, 2015.
- [26] R. Kumar and S. Chauhan, "Study on surface roughness measurement for turning of Al 7075/10/SiCp and Al 7075 hybrid composites by using response surface methodology (RSM) and artificial neural networking (ANN)," *Measurement*, vol. 65, pp. 166–180, 2015.
- [27] J. Sall, A. Lehman, M. Stephens, L. Creighton, and S. S. Jmp, *A Guide to Statistics and Data Analysis Using Jmp*, SAS Institute, Cary, NC, USA, 2012.
- [28] B. Lakhdar, Y. M. Athmane, B. Salim, and A. Haddad, "Modelling and optimization of machining parameters during hardened steel AISI D3 turning using RSM, ANN and DFA techniques: comparative study," *Journal of Mechanical Engineering and Sciences*, vol. 14, no. 2, pp. 6835–6847, 2020.
- [29] A. Chabbi, M. A. Yallese, M. Nouioua, I. Meddour, T. Mabrouki, and F. Girardin, "Modeling and optimization of turning process parameters during the cutting of polymer (POMC) based on RSM, ANN, and DF methods," *International Journal of Advanced Manufacturing Technology*, vol. 91, no. 5-8, pp. 2267–2290, 2017.